Vol 463|25 February 2010|doi:10.1038/nature08787

ARTICLES

Orm family proteins mediate sphingolipid homeostasis

David K. Breslow[1,2,3,4], Sean R. Collins[1,2,4]†, Bernd Bodenmiller[5]†, Ruedi Aebersold[5,6,7], Kai Simons[8], Andrej Shevchenko[8], Christer S. Ejsing[8,9] & Jonathan S. Weissman[1,2,4]

Despite the essential roles of sphingolipids both as structural components of membranes and critical signalling molecules, we have a limited understanding of how cells sense and regulate their levels. Here we reveal the function in sphingolipid metabolism of the *ORM* genes (known as *ORMDL* genes in humans)—a conserved gene family that includes *ORMDL3*, which has recently been identified as a potential risk factor for childhood asthma. Starting from an unbiased functional genomic approach in *Saccharomyces cerevisiae*, we identify Orm proteins as negative regulators of sphingolipid synthesis that form a conserved complex with serine palmitoyltransferase, the first and rate-limiting enzyme in sphingolipid production. We also define a regulatory pathway in which phosphorylation of Orm proteins relieves their inhibitory activity when sphingolipid production is disrupted. Changes in *ORM* gene expression or mutations to their phosphorylation sites cause dysregulation of sphingolipid metabolism. Our work identifies the Orm proteins as critical mediators of sphingolipid homeostasis and raises the possibility that sphingolipid misregulation contributes to the development of childhood asthma.

As cells grow, divide and respond to their environment, they must synthesize lipids to meet metabolic demands while ensuring the correct balance of a wide array of structurally and functionally diverse lipid species. At the same time, cells need to maintain the correct distribution of lipids within the membrane bilayers of different organelles and the plasma membrane. Regulatory mechanisms that ensure proper levels of some lipid species including sterols[1–3] and various glycerolipids[4–6] have been identified, with loss of such controls leading to a variety of disease states[1,7]. Although remarkable progress has been made in defining the protein machinery responsible for synthesizing[8,9] and transporting sphingolipids[10–13], insights into how cells sense and maintain their levels are only now emerging[14,15]. The need for precise regulation of sphingolipids may be particularly acute as, in addition to the structural roles of the terminal products, several biosynthetic intermediates—including sphingosine, ceramide and their phosphorylated derivates—are signalling molecules that participate in key physiological and pathological processes[16,17].

Our investigations into how cells achieve sphingolipid homeostasis stem from analysis of the *ORM* (or *ORMDL*) genes, which have been implicated recently in asthma. Asthma has emerged as a major health problem, with rates of childhood disease increasing markedly over the past three decades[18]. There is a strong heritable component that modulates susceptibility to asthma, and many studies have been undertaken to identify genetic risk factors[19]. A breakthrough in these efforts came with a recent genome-wide association study[20], which identified single nucleotide polymorphisms at chromosome 17q21 near the *ORMDL3* gene that confer an increased risk of childhood asthma. Subsequent studies have reproduced this finding in multiple ethnic groups[21–23]. Furthermore, the disease-associated polymorphisms have been shown to modulate expression of *ORMDL3* and the adjacent gene *GSDMB*[20,24], suggesting that dysregulation of one or both of these genes may contribute to childhood asthma. Thus genetic variants near *ORMDL3* are a widespread risk factor for developing childhood asthma that may raise the incidence of the disease by up to approximately 20% (refs 22, 25). However, translating these findings into an increased understanding of how *ORMDL3* may contribute to the pathogenesis of asthma has been hampered by the lack of information on the function of *ORM*-family genes.

Members of the *ORM* gene family encode transmembrane proteins localized in the endoplasmic reticulum (ER) and include two genes in the budding yeast *S. cerevisiae* (*ORM1/2*) and three genes in humans (*ORMDL1/2/3*)[26]. The Orm proteins have no known functional domains, and little is known about their cellular role; however, they are strongly conserved and have been proposed to share a common function[26]. Here we use a combination of global and targeted studies to identify Orm proteins as homeostatic regulators of the first and rate-limiting step in sphingolipid biosynthesis.

Orm1/2 negatively regulate sphingolipid synthesis

We began our investigation of *S. cerevisiae ORM1* and *ORM2* by using a global approach to characterize gene function based on large-scale measurements of genetic interactions, termed epistatic mini-array profiles (E-MAPs)[27]. In this strategy, the function of a given gene can be inferred without a priori hypotheses by comparing the spectrum of genetic interactions resulting from mutation of that gene with interaction patterns caused by mutations in other genes of defined function. When we compared the genetic interaction profile resulting from deletion of *ORM2* with those obtained for a collection of more than 1,400 yeast mutants in a study focused on ER biology (manuscript in preparation and ref. 27), we observed a strong anti-correlation with the interaction patterns seen for hypomorphic alleles that reduce expression of *LCB1* and *LCB2* (*lcb1-DAmP* and *lcb2-DAmP*[27]), thus suggesting that *ORM2* and *LCB1/2* have opposing cellular roles (Fig. 1a and Supplementary Information). We also

[1]Department of Cellular and Molecular Pharmacology, [2]Howard Hughes Medical Institute, [3]Graduate Program in Chemistry and Chemical Biology, [4]The California Institute for Quantitative Biomedical Research, University of California, San Francisco, 1700 4th Street, San Francisco, California 94158, USA. [5]Institute of Molecular Systems Biology, ETH Zurich, 8093 Zurich, Switzerland. [6]Institute for Systems Biology, Seattle, Washington 98103, USA. [7]Faculty of Science, University of Zurich, 8057 Zurich, Switzerland. [8]Max Planck Institute of Molecular Cell Biology and Genetics, Pfotenhauerstrasse 108, 01307 Dresden, Germany. [9]Department of Biochemistry and Molecular Biology, University of Southern Denmark, Campusvej 55, 5230 Odense, Denmark. †Present addresses: Chemical and Systems Biology, Bio-X Program, Stanford University, Stanford, California 94305, USA (S.R.C.); Department of Microbiology and Immunology, Baxter Laboratory in Genetic Pharmacology, Stanford University, 269 Campus Drive, Stanford, California 94305, USA (B.B.).

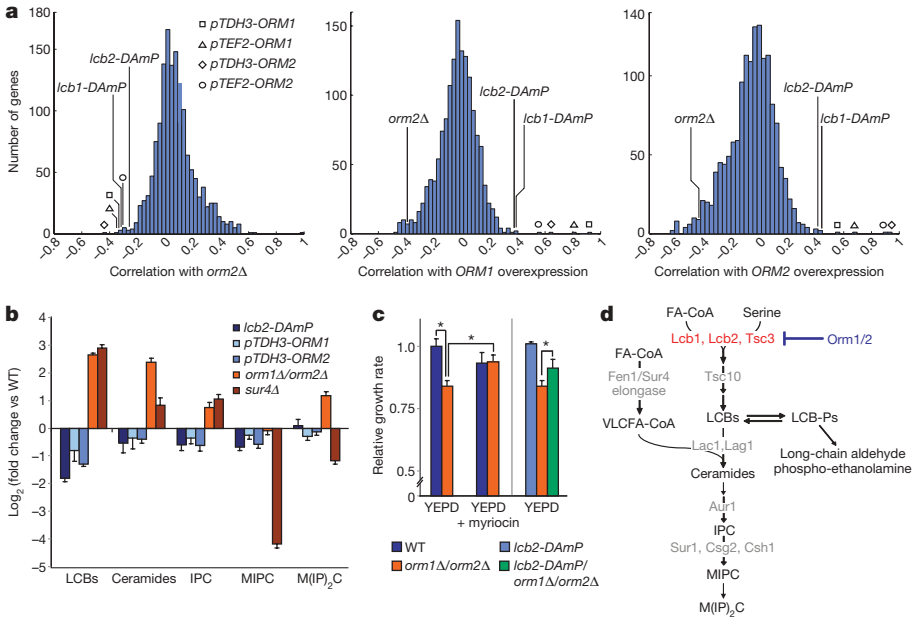

Figure 1 | Orm1/2 are negative regulators of sphingolipid synthesis. **a**, Genetic interaction (E-MAP) profiles were generated for strains containing *ORM2* deletion, *ORM1* overexpression and *ORM2* overexpression alleles (*orm2*Δ, *pTDH3-ORM1* and *pTEF2-ORM1*, and *pTDH3-ORM2* and *pTEF2-ORM2*, respectively). Correlations between the E-MAP profiles of these strains and those of more than 1,400 other yeast mutants are shown in histograms (see Methods and Supplementary Information). **b**, Lipids were extracted from the indicated strains and analysed using a global mass spectrometry approach[30]. Amounts of the indicated metabolites are shown relative to wild type (WT; average ± s.d., $n = 4$; see Methods and Supplementary Information). **c**, Logarithmic-phase growth rates for the indicated strains were measured in standard media (YEPD) or media supplemented with myriocin at 150 ng ml^{-1}. Growth rates (average ± s.d., $n \geq 3$) are shown normalized to wild type; asterisks denote statistical significance ($P < 0.05$). **d**, Schematic of the sphingolipid biosynthesis pathway in *S. cerevisiae*, with selected metabolites and genes indicated. FA-CoA, fatty acid co-enzyme A; LCB-Ps, long-chain base phosphates; IPC, inositolphosphorylceramide; MIPC, mannosyl-inositolphosphorylceramide; MIP_2C, mannosyl-diinositolphosphorylceramide; VLCFA-CoA, very long-chain fatty acid co-enzyme A.

examined the genetic interactions that result from overexpression of *ORM1* or *ORM2* by using the strong promoters *pTDH3* and *pTEF2*, as it was shown that the asthma-associated polymorphisms near *ORMDL3* are associated with increased expression of this gene[20,24]. Overexpression of *ORM1* or *ORM2* produced a pattern of genetic interactions that was highly correlated with those seen for the *lcb1-DAmP* and *lcb2-DAmP* strains, indicating that increased Orm expression phenocopies reduced Lcb1/2 activity (Fig. 1a).

LCB1 and *LCB2* encode serine palmitoyltransferase, an essential heterodimeric enzyme that catalyses the first and rate-limiting step in sphingolipid biosynthesis[9,28]. The synthesis of sphingolipids begins in the ER, where two classes of lipid metabolite, long-chain bases (LCBs) and very long-chain fatty acids, are formed (Fig. 1d). LCBs are produced by the condensation of serine with fatty acids by serine palmitoyltransferase (Lcb1/2 in yeast and SPTLC1/2/3 in mammals), followed by Tsc10-mediated reduction[8,9,29]. LCBs can then be phosphorylated or *N*-acylated with very long-chain fatty acids to form long-chain base phosphates or ceramides, respectively, with the latter undergoing further modification to generate complex sphingolipids (Fig. 1d).

Thus, our E-MAP data showing a correlation between increased *ORM* expression and decreased *LCB1/2* function implicate the Orm proteins as negative regulators of sphingolipid synthesis and highlight the reaction performed by Lcb1/2 as the possible step in the pathway at which Orm1/2 may act (Fig. 1a, d). We therefore examined the effects of altering Orm levels on cellular lipid composition using a mass-spectrometry-based global lipidomic technique[30]. In agreement with the genetic interaction data, overexpression of *ORM1* or *ORM2* resulted in changes to the lipidome, including reduced levels of LCBs and ceramides, which closely resembled those seen for the *lcb2-DAmP* mutant (Fig. 1b and Supplementary Information). Conversely, cells deleted for *ORM1/2* had highly increased levels of LCBs and ceramides. In principle, this accumulation of LCBs caused by deletion of *ORM1/2* could result from a failure to consume these species by reaction with very long-chain fatty acids to form ceramides, as is seen when *SUR4* is deleted (Fig. 1b and ref. 30). However, in contrast to the *sur4*Δ strain, the increased LCB levels in the *orm1*Δ/*orm2*Δ strain are also accompanied by increased amounts of the terminal sphingolipid mannosyl-diinositolphosphorylceramide. Thus, *ORM1/2* deletion causes increased flux throughout the sphingolipid pathway. This increased flux is also the primary cause of the growth defect seen in *orm1*Δ/*orm2*Δ cells, as artificially decreasing Lcb1/2 activity, either through the use of myriocin, a drug that specifically inhibits Lcb1/2 (ref. 31), or through the *lcb2-DAmP* allele, significantly suppresses the growth defect caused by loss of *ORM1/2* (Fig. 1c).

A complex with Orm1/2, Lcb1/2 and Sac1

We next explored how Orm proteins modulate sphingolipid production by identifying proteins bound by Orm1 and Orm2 *in vivo*. Isolation of functional 3×Flag-tagged forms of Orm1 and Orm2 expressed from their endogenous loci revealed a previously uncharacterized, roughly stoichiometric complex (Fig. 2a). Mass spectrometry showed that this complex comprises the serine palmitoyltransferase proteins Lcb1, Lcb2 and Tsc3, in addition to the phosphoinositide phosphatase Sac1 (ref. 32) (Supplementary Table 1). To characterize physical interactions among these proteins further, we used a 3×Flag-tagged form of Lcb1 that is able to rescue the inviability seen upon loss of *LCB1* (although this allele does exhibit mild sensitivity to myriocin). Purification of 3×Flag–Lcb1 yielded the same components seen in the Orm1/2 pull-downs (Fig. 2b), indicating that the Orm-associated proteins are likely to exist in a single complex. Orm proteins and potentially their binding partners may also form higher-order oligomers, as we detected Orm2 co-immunoprecipitation with 3×Flag–Orm1 (and vice versa) and self-association of differently tagged copies of the same Orm protein (Fig. 2a and see later).

The presence of Sac1 in association with Lcb1/2 suggests a new connection between this phosphoinositide phosphatase and sphingolipid biosynthesis. Deletion of *SAC1* leads to increased levels of

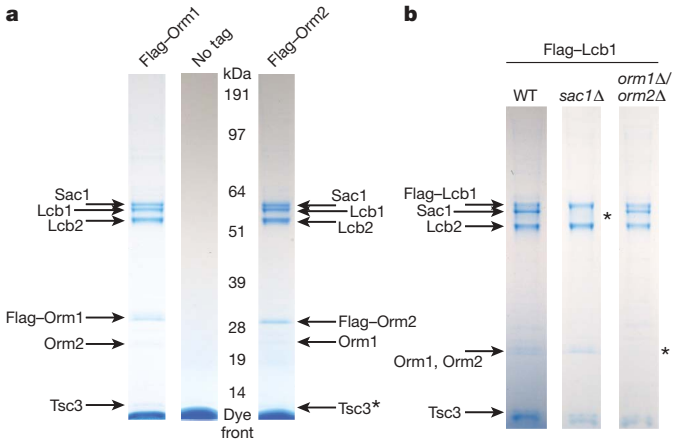

Figure 2 | Orm proteins form a complex with serine palmitoyltransferase. **a**, Colloidal-stained gels are shown for proteins eluted after affinity purifications from strains expressing 3×Flag–Orm1 or 3×Flag–Orm2, or from an untagged control strain. Immunoprecipitated proteins were identified by mass spectrometry (Supplementary Table 1; asterisk indicates the partly obscured protein Tsc3, whose presence was confirmed by mass spectrometry). **b**, Affinity purifications of 3×Flag–Lcb1 from wild-type, *sac1*Δ and *orm1*Δ/*orm2*Δ strains were performed as in **a**. Asterisks indicate bands that are lost in deletion backgrounds.

LCBs (Supplementary Fig. 1a and ref. 33) and resistance to the Lcb1/2 inhibitor myriocin (Supplementary Fig. 1b). This resistance was also seen in cells expressing the *sac1–8* (ref. 34) catalytically inactive mutant of *SAC1*. Additionally, we found that Sac1 and Orm1/2 bind independently to Lcb1/2 (Fig. 2b) and that *SAC1* and *ORM1/2* deletions exhibit synthetic lethality (Supplementary Fig. 1c). These findings together suggest that Sac1 modulates serine palmitoyltransferase activity directly, but in a mode distinct from Orm1/2.

Finally, we showed that the functional complex between Orm proteins and serine palmitoyltransferase is conserved in human cells. Immunoprecipitations from HEK293T cells expressing 3×Flag-tagged ORMDL3 led to a prominent SPTLC1 band detected by western blot (Fig. 3a). Furthermore, we found that simultaneous knockdown by RNA interference of *ORMDL1/2/3* in HeLa cells causes an approximately threefold increase in ceramide levels (Fig. 3b, Supplementary Fig. 2 and Supplementary Information).

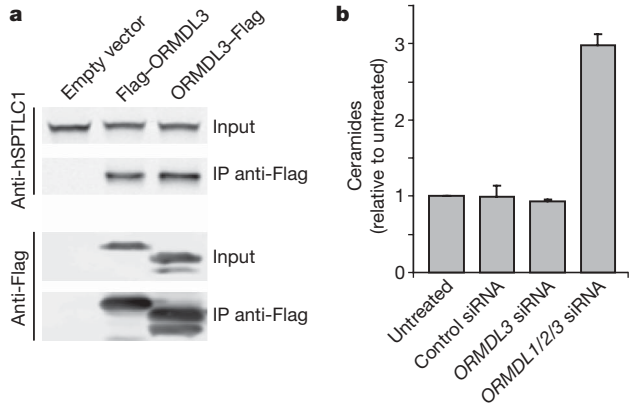

Figure 3 | *ORM* gene function is conserved in human cells. **a**, HEK293T cells were transfected with either an empty vector or a vector encoding ORMDL3 fused to the 3×Flag epitope (N- or carboxy-terminal fusion). Immunoprecipitations with anti-Flag agarose were analysed by western blot against human serine palmitoyltransferase (anti-hSPTLC1) and against the Flag epitope (anti-Flag). **b**, HeLa cells were transfected with short interfering RNAs (siRNAs) directed against the indicated genes. After 72 h, cells were collected and their lipids were analysed by mass spectrometry. Ceramide levels normalized to phosphatidylcholine are shown (moles of ceramide per mole of phosphatidylcholine, relative to untreated cells; average ± s.d., $n = 3$).

Together, these results establish that Orm proteins are components of a novel and conserved protein complex, which we term the SPOTS complex (serine palmitoyltransferase, Orm1/2, Tsc3, and Sac1). Additionally, our data indicate that Orm1/2 negatively regulate sphingolipid synthesis by acting directly on Lcb1/2 (for example by altering Lcb1/2 catalytic activity, accessibility of substrates to the enzyme or its subcellular localization).

Homeostatic regulation of Orm1/2 activity

Why would cells include negative regulators of serine palmitoyltransferase, Orm1/2, as core components of this essential enzyme complex? This seemingly paradoxical arrangement prompted us to investigate whether Orm-mediated inhibition of LCB production might be regulated in response to changes in the cellular need for sphingolipid synthesis. We therefore examined how *ORM1/2* deletion affects sensitivity to the Lcb1/2 inhibitor myriocin. Growth in the presence of myriocin is strongly dependent on the cellular capacity for LCB production, as the *lcb2-DAmP* strain is highly sensitive to myriocin (Fig. 4a); in addition, *SAC1* deletion, which leads to increased LCB levels, confers myriocin resistance (Fig. 4a). Thus, naively, we might expect deletion of *ORM1/2* also to confer pronounced resistance to this drug. However, we observed that wild-type and *orm1*Δ/*orm2*Δ strains exhibit comparable growth in the presence of myriocin (Fig. 4a). Thus, loss of *ORM1/2* strongly affects cell growth under standard conditions but has little apparent effect when sphingolipid synthesis is disrupted, suggesting that Orm1/2 may be inactivated in response to myriocin treatment.

To investigate this possibility further, we compared the effects of myriocin on the LCB levels of wild-type and *orm1*Δ/*orm2*Δ strains. As described earlier, the *ORM1/2* deletion strain exhibits highly increased LCB levels in the absence of myriocin. However, with increasing doses of myriocin, LCB levels in the *orm1*Δ/*orm2*Δ strain decrease strongly and approximately converge with those of the wild-type strain (Fig. 4b), supporting our growth data indicating that Orm1/2 may be inactivated in response to myriocin treatment (Fig. 4a). Interestingly, we also found that wild-type cells maintain roughly constant LCB levels even at intermediate concentrations of myriocin (up to about 40 ng ml^{-1}). This robustness is not due to a failure of myriocin to affect Lcb1/2 at these concentrations, as LCB levels in the *orm1*Δ/*orm2*Δ strain are reduced strongly by the same drug concentrations (Fig. 4b; for further evidence see Fig. 4d). Rather, these results indicate that progressive inactivation of Orm1/2 may provide cells with a homeostatic mechanism to maintain nearly constant sphingolipid output in the face of increasing Lcb1/2 inhibition. Consistent with this hypothesis, LCB levels in the wild-type strain begin to decline only at myriocin concentrations where Orm-mediated inhibition of LCB synthesis appears to be fully relieved, as evidenced by convergence of wild-type and *orm1*Δ/*orm2*Δ LCB levels (Fig. 4b).

Orm1/2 regulation by phosphorylation

We next investigated the mechanism by which Orm1/2 activity might be decreased in response to myriocin treatment. Growth in myriocin did not alter Orm1/2 expression levels (Fig. 4c and Supplementary Fig. 7) or abolish their ability to interact with Lcb1/2 and Sac1 (Supplementary Fig. 3). However, we observed a notable reduction in localization of green fluorescent protein (GFP)–Orm2 to the cortical but not perinuclear ER after treatment with myriocin (Supplementary Fig. 4), raising the possibility that changes in subcellular localization contribute to regulation of SPOTS complex activity. We also found a strong reduction in Orm protein co-immunoprecipitation in cells treated with myriocin (Fig. 4c), both for Orm1–Orm2 interaction and for self-association of Orm1 and of Orm2. A weak reduction in Orm–Lcb1 binding was also observed in response to myriocin (Fig. 4c). These findings suggest a model in which Orm–Lcb1/2 sub-complexes can self-associate into higher-order oligomers in a

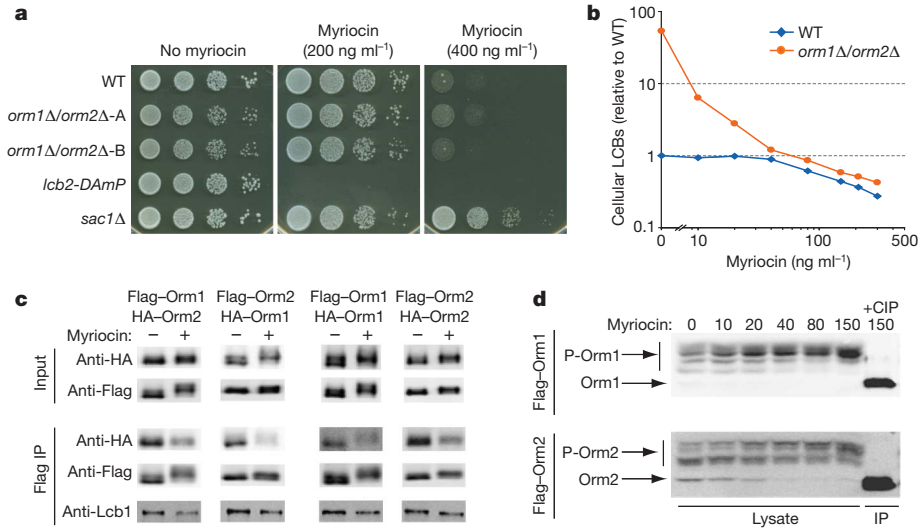

Figure 4 | Orm1/2 are regulated in response to disruption of sphingolipid synthesis. a, Serial dilutions of the indicated strains were spotted on plates containing 0, 200 or 400 ng ml^{-1} myriocin and imaged after growth for 24–48 h. **b**, LCBs were extracted and analysed from wild-type and *ORM1/2* deletion strains grown in media supplemented with the indicated concentrations of myriocin. The combined amounts of C18 dihydrosphingosine and C18 phytosphingosine are shown (relative to wild-type LCB levels in the absence of myriocin; average of $n \geq 2$ experiments). **c**, Native immunoprecipitations of 3×Flag-tagged Orm1 and Orm2 were performed from strains grown in standard media or media supplemented with 150 ng ml^{-1} myriocin, and analysed by western blot. The indicated strains also expressed 3×HA–Orm1/2 from their endogenous loci (diploid strains were used to examine self-association of Orm1 and Orm2). **d**, Lysates were prepared from yeast expressing 3×Flag–Orm1/2 after growth in media containing the indicated concentrations of myriocin. Western blots show phosphorylated forms of 3×Flag–Orm1 (P-Orm1) and 3×Flag–Orm2 (P-Orm2) after separation on phosphate-affinity gels[35]. An immunoprecipitated (IP) sample treated with calf intestine phosphatase (CIP) shows the position of unphosphorylated Orm1/2.

manner that is inhibited in response to disruptions to sphingolipid synthesis.

We also detected in our Orm1/2 co-immunoprecipitations a slight shift in the electrophoretic mobility of Orm1 isolated from myriocin-treated cells, indicating that Orm proteins may be post-translationally modified (see Fig. 4c, Flag–Orm1 and haemagglutinin (HA)–Orm1 inputs). Analysis of 3×Flag–Orm1 and 3×Flag–Orm2 in SDS–polyacrylamide gel electrophoresis (SDS–PAGE) gels that incorporated a phosphate-binding agent to improve the separation of phosphorylated species[35] resolved multiple phosphorylated forms for both Orm1 and Orm2 that collapsed to faster-migrating species upon phosphatase treatment (Fig. 4d). Importantly, growth in myriocin induced a dose-dependent shift to more highly phosphorylated forms, and this response occurred over the same concentrations of myriocin that led to homeostatic inactivation of Orm1/2, as determined by measurements of LCBs (compare Fig. 4b and 4d). We also observed increased Orm1/2 phosphorylation after shutting off expression of downstream sphingolipid synthetic enzymes such as Tsc10 or Lag1 (in a *lac1*Δ background; Supplementary Fig. 5), further indicating that phosphorylation of Orm proteins is a homeostatic response to disruption of sphingolipid production (see Fig. 5c). Finally, we did not observe substantial changes in Orm1/2 phosphorylation upon shutting off expression of *AUR1* or *CSG2* (Supplementary Fig. 5), thus providing preliminary evidence that a metabolite upstream of these enzymes, such as ceramide, is an intermediate whose levels are sensed to regulate Orm1/2 activity.

To test our phosphorylation-mediated feedback model directly, we identified residues of Orm1 and Orm2 that are phosphorylated. Through a combination of targeted mutagenesis and mass spectrometry, we found several sites of Orm1 and Orm2 phosphorylation in the amino-terminal regions of these proteins (Fig. 5a and Supplementary Fig. 6). Importantly, mutation of these sites to alanine blocks formation of the slower-migrating phosphorylated species seen in phosphate-affinity gels (Fig. 5a). This loss of phosphorylation is unlikely to be due to these mutations resulting in non-functional Orm proteins, as the phospho-mutants are expressed at levels comparable to wild type and rescue the slow growth of the *orm1*Δ/*orm2*Δ strain (Supplementary Fig. 7 and data not shown). Furthermore, immunoprecipitations of phospho-mutant Orm1 and Orm2 revealed that these proteins not only maintain the ability to interact with Lcb1 and each other, but that blocking phosphorylation prevents the change in higher-order assembly of the SPOTS complex normally seen in response to myriocin (Fig. 5b). Thus Orm1/2 phosphorylation appears to be the event that triggers dynamic regulation of SPOTS complex oligomerization.

We next investigated the *in vivo* role of Orm1/2 phosphorylation. Consistent with a basal level of Orm1/2 phosphorylation that is important for steady-state LCB production, we observed a substantial (twofold) reduction in LCB levels in the *ORM1/2* phospho-mutant strain under standard growth conditions (Fig. 5d). Furthermore, we found that this strain is highly sensitive to treatment with myriocin (Fig. 5e). This result therefore confirms a key prediction of our homeostatic model and indicates that although cells may possess additional mechanisms to regulate sphingolipid biosynthesis, such pathways cannot compensate for disruption of the critical feedback control provided by Orm1/2. Thus, Orm proteins are dynamic negative regulators of serine palmitoyltransferase, whose inhibitory activity is dependent on adequate levels of downstream sphingolipids (Fig. 5c).

Discussion

Our studies identify Orm proteins as homeostatic regulators of sphingolipid metabolism and demonstrate that alteration of these controls leads to misregulation of sphingolipid production (Fig. 5c). Specifically, loss of the Orm1/2-mediated brake on serine palmitoyltransferase activity results in toxic accumulation of sphingolipids, whereas mutations that prevent this brake from being removed render cells unable to survive disruptions to sphingolipid synthesis.

A phosphorylation-based feedback loop provides a mechanistic basis for homeostatic regulation of sphingolipid production and exhibits several features that make it well suited to control sphingolipid levels precisely. First, phosphorylation of a direct regulator of serine palmitoyltransferase may enable cells to respond rapidly to changing environments. Second, Orm1/2 exhibit partial phosphorylation under standard growth conditions, which may position the

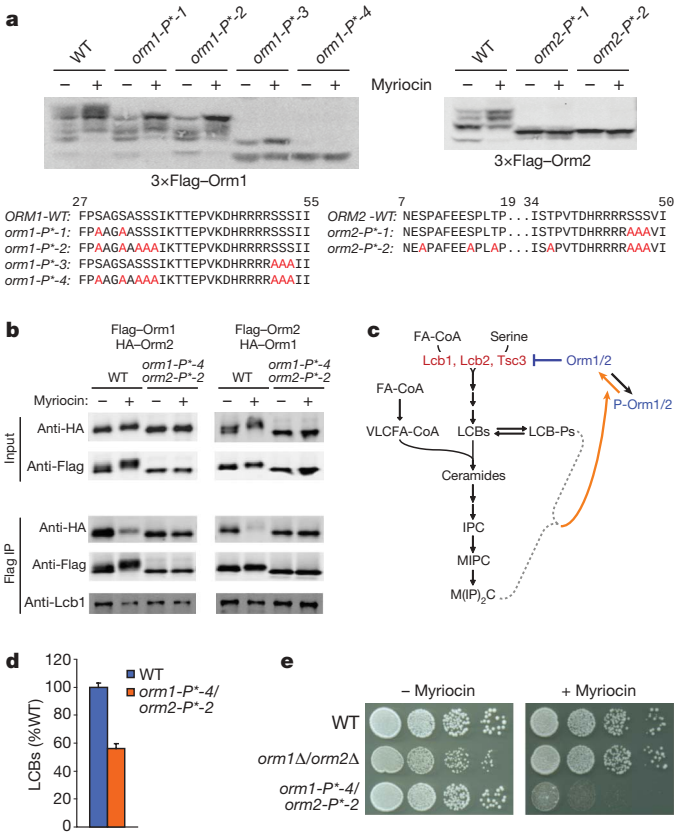

Figure 5 | Mutation of phosphorylated Orm1/2 residues impairs sphingolipid homeostasis. a, Lysates were prepared from strains expressing wild-type or phospho-site mutant 3×Flag–Orm1 or 3×Flag–Orm2 after growth in standard media or media supplemented with 150 ng ml^{-1} myriocin. Western blots are shown after protein separation on phosphate-affinity gels. Residues mutated to alanine in the indicated phospho-mutants are highlighted in red below. **b**, Native immunoprecipitations of 3×Flag-tagged wild-type or phospho-mutant Orm1 and Orm2 were performed from strains expressing wild-type or phospho-mutant 3×HA–Orm1/2 after growth in standard media or media supplemented with 100 ng ml^{-1} myriocin. Western blots were analysed as in Fig. 4c. **c**, Model for homeostatic regulation of Orm1/2, in which Orm proteins act as negative regulators of serine palmitoyltransferase (Lcb1, Lcb2 and Tsc3), whose inhibitory activity is dependent on levels of downstream sphingolipids. See Fig. 1d for abbreviations used. **d**, LCBs were extracted and analysed from wild-type and 3×Flag-tagged *ORM1/2* double phospho-mutant strains grown in standard media. Data were analysed as in Fig. 4b (average ± s.d., $n = 3$). **e**, Serial dilutions of wild-type, *ORM1/2* deletion and 3×Flag-tagged *ORM1/2* double-phospho-mutant strains were spotted on plates with 0 or 280 ng ml^{-1} myriocin and imaged after growth for 24–36 h.

Orm1/2-based sphingolipid rheostat for maximal sensitivity to changes in lipid metabolism. Furthermore, multi-site phosphorylation of Orm1 and Orm2 has the potential to generate several distinct and stable phospho-states, which may provide cells with a graded mechanism to adjust lipid production finely to match cellular needs. Finally, several phosphorylation sites may also render Orm1/2 responsive to multiple physiological or metabolic cues.

Our identification of the SPOTS complex reveals a new mechanism by which cells may be able to coordinate a variety of important secretory pathway processes. Although a link between sphingolipids and phosphoinositides has been appreciated for some time[29,33,36], we provide evidence that the phosphoinositide phosphatase Sac1 directly modulates sphingolipid metabolism, as it is associated physically with serine palmitoyltransferase. These results are of particular interest given the role of phosphoinositides, including the Sac1 substrate phosphatidylinositol-4-phosphate, in the trafficking of both proteins and sphingolipids from the ER and Golgi apparatus[10,11,32]. Additionally, changes in Sac1 localization from the ER to the Golgi have been shown in both yeast and mammals to regulate protein flux through the secretory pathway in response to nutrient levels[37]. We therefore suggest that the SPOTS complex may represent a dynamic coordinating centre that couples changes in sphingolipid and nutrient levels to the activity and localization of key enzymes of lipid metabolism and trafficking. This model is consistent with our finding that Orm proteins self-associate in a regulated fashion and with evidence that mammalian serine palmitoyltransferase is part of a high-molecular-mass complex[38].

Finally, our characterization of *ORM* gene function provides a framework for investigating whether alterations in *ORMDL3* activity and sphingolipid metabolism play a role in the pathogenesis of asthma. Several studies support a role for sphingolipids such as ceramide and sphingosine-1-phosphate in asthma-associated inflammatory processes, including mast-cell degranulation, airway hyper-responsiveness and immune-cell trafficking[39–43]. Our findings now link this growing body of evidence to the identification of single nucleotide polymorphisms near *ORMDL3* that are associated with childhood asthma[20]. Specifically, our observation that altered Orm levels strongly impact sphingolipid metabolism raises the testable hypothesis that misregulation of sphingolipids may have a direct and causative role in the development of asthma. A broader potential role for sphingolipids in inflammatory disease is also suggested by reports that single nucleotide polymorphisms near *ORMDL3* are associated with Crohn's disease[44], type I diabetes[45] and primary biliary cirrhosis[46]. Finally, the existence of a rich set of pharmacological tools targeting the sphingolipid pathway[31] raises the possibility of therapeutic intervention to counteract the potential effects of changes in *ORMDL3* activity.

METHODS SUMMARY

Phosphorylation analysis by phosphate-affinity SDS–PAGE. Lysates for phosphorylation analysis were prepared by pelleting and immediately resuspending logarithmically growing yeast in SDS lysis buffer (50 mM Tris-Cl, pH 6.8, 2% SDS, 10% glycerol) with protease inhibitors (Complete EDTA-free Protease Inhibitor Tablets; Roche) at 65 °C. SDS–PAGE gels with phosphate affinity reagent[35] (synthesized according to standard synthetic procedures) were prepared with a 7.5% acrylamide resolving gel with 50 μM $MnCl_2$ and 25 μM phosphate affinity reagent (375 mM Tris, pH 8.8, 0.1% SDS). Gels were run at 70 V for 2.5 h, rinsed twice for 5 min in transfer buffer with 1 mM EDTA and rinsed twice more for 5 min in transfer buffer without EDTA before transfer to nitrocellulose membranes.

Western blots. Proteins were transferred from SDS–PAGE gels to nitrocellulose membranes and probed for proteins of interest by using standard western blot procedures. Antibodies used were as follows: rabbit anti-Flag (Sigma Aldrich), mouse anti-Flag (M2; Sigma Aldrich), mouse anti-HA antibodies 12CA5 (Roche) and HA.11 (Covance), mouse anti-yPgk1 (Molecular Probes), rabbit anti-yLcb1 (raised against peptide antigen SYIKKSHHDDPYRTTC; Abgent), mouse anti-hSPTLC1 (Becton Dickinson) and rabbit anti-ORMDL1/2/3 (raised against peptide antigen KGTPFETPDQGKARLC; Abgent). Western blots were scanned using an Odyssey fluorescent scanner (Li-Cor Biosciences).

Full Methods and any associated references are available in the online version of the paper at www.nature.com/nature.

Received 23 August; accepted 17 December 2009.

1. Brown, M. S. & Goldstein, J. L. Cholesterol feedback: from Schoenheimer's bottle to Scap's MELADL. *J. Lipid Res.* **50** (suppl.), S15–S27 (2009).
2. Hampton, R. Y. & Garza, R. M. Protein quality control as a strategy for cellular regulation: lessons from ubiquitin-mediated regulation of the sterol pathway. *Chem. Rev.* **109**, 1561–1574 (2009).
3. Burg, J. S. *et al.* Insig regulates HMG-CoA reductase by controlling enzyme phosphorylation in fission yeast. *Cell Metab.* **8**, 522–531 (2008).
4. Loewen, C. J. *et al.* Phospholipid metabolism regulated by a transcription factor sensing phosphatidic acid. *Science* **304**, 1644–1647 (2004).
5. Martin, C. E., Oh, C. S. & Jiang, Y. Regulation of long chain unsaturated fatty acid synthesis in yeast. *Biochim. Biophys. Acta* **1771**, 271–285 (2007).
6. Kurat, C. F. *et al.* Cdk1/Cdc28-dependent activation of the major triacylglycerol lipase Tgl4 in yeast links lipolysis to cell-cycle progression. *Mol. Cell* **33**, 53–63 (2009).
7. Fischer, J. *et al.* The gene encoding adipose triglyceride lipase (PNPLA2) is mutated in neutral lipid storage disease with myopathy. *Nature Genet.* **39**, 28–30 (2007).

8. Dickson, R. C., Sumanasekera, C. & Lester, R. L. Functions and metabolism of sphingolipids in *Saccharomyces cerevisiae. Prog. Lipid Res.* **45,** 447–465 (2006).
9. Cowart, L. A. & Obeid, L. M. Yeast sphingolipids: recent developments in understanding biosynthesis, regulation, and function. *Biochim. Biophys. Acta* **1771,** 421–431 (2007).
10. Hanada, K. *et al.* Molecular machinery for non-vesicular trafficking of ceramide. *Nature* **426,** 803–809 (2003).
11. D'Angelo, G. *et al.* Glycosphingolipid synthesis requires FAPP2 transfer of glucosylceramide. *Nature* **449,** 62–67 (2007).
12. Kumagai, K., Kawano, M., Shinkai-Ouchi, F., Nishijima, M. & Hanada, K. Interorganelle trafficking of ceramide is regulated by phosphorylation-dependent cooperativity between the PH and START domains of CERT. *J. Biol. Chem.* **282,** 17758–17766 (2007).
13. Klemm, R. W. *et al.* Segregation of sphingolipids and sterols during formation of secretory vesicles at the trans-Golgi network. *J. Cell Biol.* **185,** 601–612 (2009).
14. Aronova, S. *et al.* Regulation of ceramide biosynthesis by TOR complex 2. *Cell Metab.* **7,** 148–158 (2008).
15. Vacaru, A. M. *et al.* Sphingomyelin synthase-related protein SMSr controls ceramide homeostasis in the ER. *J. Cell Biol.* **185,** 1013–1027 (2009).
16. Hannun, Y. A. & Obeid, L. M. Principles of bioactive lipid signalling: lessons from sphingolipids. *Nature Rev. Mol. Cell Biol.* **9,** 139–150 (2008).
17. Lebman, D. A. & Spiegel, S. Cross-talk at the crossroads of sphingosine-1-phosphate, growth factors, and cytokine signaling. *J. Lipid Res.* **49,** 1388–1394 (2008).
18. Akinbami, L. J., Moorman, J. E., Garbe, P. L. & Sondik, E. J. Status of childhood asthma in the United States, 1980–2007. *Pediatrics* **123** (suppl. 3), S131–S145 (2009).
19. Vercelli, D. Discovering susceptibility genes for asthma and allergy. *Nature Rev. Immunol.* **8,** 169–182 (2008).
20. Moffatt, M. F. *et al.* Genetic variants regulating ORMDL3 expression contribute to the risk of childhood asthma. *Nature* **448,** 470–473 (2007).
21. Galanter, J. *et al.* ORMDL3 gene is associated with asthma in three ethnically diverse populations. *Am. J. Respir. Crit. Care Med.* **177,** 1194–1200 (2008).
22. Wu, H. *et al.* Genetic variation in ORM1-like 3 (ORMDL3) and gasdermin-like (GSDML) and childhood asthma. *Allergy* **64,** 629–635 (2009).
23. Bouzigon, E. *et al.* Effect of 17q21 variants and smoking exposure in early-onset asthma. *N. Engl. J. Med.* **359,** 1985–1994 (2008).
24. Verlaan, D. J. *et al.* Allele-specific chromatin remodeling in the ZPBP2/GSDMB/ORMDL3 locus associated with the risk of asthma and autoimmune disease. *Am. J. Hum. Genet.* **85,** 377–393 (2009).
25. Tavendale, R., Macgregor, D. F., Mukhopadhyay, S. & Palmer, C. N. A polymorphism controlling ORMDL3 expression is associated with asthma that is poorly controlled by current medications. *J. Allergy Clin. Immunol.* **121,** 860–863 (2008).
26. Hjelmqvist, L. *et al.* ORMDL proteins are a conserved new family of endoplasmic reticulum membrane proteins. *Genome Biol.* **3,** doi:10.1186/gb-2002-3-6-research0027 (2002).
27. Schuldiner, M. *et al.* Exploration of the function and organization of the yeast early secretory pathway through an epistatic miniarray profile. *Cell* **123,** 507–519 (2005).
28. Hanada, K. Serine palmitoyltransferase, a key enzyme of sphingolipid metabolism. *Biochim. Biophys. Acta* **1632,** 16–30 (2003).
29. Beeler, T. *et al.* The *Saccharomyces cerevisiae* TSC10/YBR265w gene encoding 3-ketosphinganine reductase is identified in a screen for temperature-sensitive suppressors of the Ca^{2+}-sensitive *csg2Δ* mutant. *J. Biol. Chem.* **273,** 30688–30694 (1998).
30. Ejsing, C. S. *et al.* Global analysis of the yeast lipidome by quantitative shotgun mass spectrometry. *Proc. Natl Acad. Sci. USA* **106,** 2136–2141 (2009).
31. Delgado, A., Casas, J., Llebaria, A., Abad, J. L. & Fabrias, G. Inhibitors of sphingolipid metabolism enzymes. *Biochim. Biophys. Acta* **1758,** 1957–1977 (2006).
32. Strahl, T. & Thorner, J. Synthesis and function of membrane phosphoinositides in budding yeast, *Saccharomyces cerevisiae. Biochim. Biophys. Acta* **1771,** 353–404 (2007).
33. Brice, S. E., Alford, C. W. & Cowart, L. A. Modulation of sphingolipid metabolism by the phosphatidylinositol-4-phosphate phosphatase Sac1p through regulation of phosphatidylinositol in *Saccharomyces cerevisiae. J. Biol. Chem.* **284,** 7588–7596 (2009).
34. Kearns, B. G. *et al.* Essential role for diacylglycerol in protein transport from the yeast Golgi complex. *Nature* **387,** 101–105 (1997).
35. Kinoshita, E., Kinoshita-Kikuta, E., Takiyama, K. & Koike, T. Phosphate-binding tag, a new tool to visualize phosphorylated proteins. *Mol. Cell. Proteomics* **5,** 749–757 (2006).
36. Tabuchi, M., Audhya, A., Parsons, A. B., Boone, C. & Emr, S. D. The phosphatidylinositol 4,5-biphosphate and TORC2 binding proteins Slm1 and Slm2 function in sphingolipid regulation. *Mol. Cell. Biol.* **26,** 5861–5875 (2006).
37. Blagoveshchenskaya, A. & Mayinger, P. SAC1 lipid phosphatase and growth control of the secretory pathway. *Mol. Biosyst.* **5,** 36–42 (2009).
38. Hornemann, T., Wei, Y. & von Eckardstein, A. Is the mammalian serine palmitoyltransferase a high-molecular-mass complex? *Biochem. J.* **405,** 157–164 (2007).
39. Rivera, J., Proia, R. L. & Olivera, A. The alliance of sphingosine-1-phosphate and its receptors in immunity. *Nature Rev. Immunol.* **8,** 753–763 (2008).
40. Ammit, A. J. *et al.* Sphingosine 1-phosphate modulates human airway smooth muscle cell functions that promote inflammation and airway remodeling in asthma. *FASEB J.* **15,** 1212–1214 (2001).
41. Masini, E. *et al.* Ceramide: a key signaling molecule in a guinea pig model of allergic asthmatic response and airway inflammation. *J. Pharmacol. Exp. Ther.* **324,** 548–557 (2008).
42. Ryan, J. J. & Spiegel, S. The role of sphingosine-1-phosphate and its receptors in asthma. *Drug News Perspect.* **21,** 89–96 (2008).
43. Idzko, M. *et al.* Local application of FTY720 to the lung abrogates experimental asthma by altering dendritic cell function. *J. Clin. Invest.* **116,** 2935–2944 (2006).
44. Barrett, J. C. *et al.* Genome-wide association defines more than 30 distinct susceptibility loci for Crohn's disease. *Nature Genet.* **40,** 955–962 (2008).
45. Barrett, J. C. *et al.* Genome-wide association study and meta-analysis find that over 40 loci affect risk of type 1 diabetes. *Nature Genet.* **41,** 703–707 (2009).
46. Hirschfield, G. M. *et al.* Primary biliary cirrhosis associated with HLA, IL12A, and IL12RB2 variants. *N. Engl. J. Med.* **360,** 2544–2555 (2009).

Supplementary Information is linked to the online version of the paper at www.nature.com/nature.

Acknowledgements We acknowledge A. Falick, S. Zhou and D. King for identification of proteins by mass spectrometry; M. Schuldiner and S. Wang for E-MAP data collection; D. Fiedler and K. Shokat for providing the phosphate-binding acrylamide reagent; E. Griffis and M. D'Ambrosio for assistance with fluorescence microscopy; N. Ingolia for a codon-optimized mCherry-tagging plasmid; E. Burchard and J. Galanter for discussions of asthma genetics; I. Poser and A. Hyman for advice and providing the HeLa-Kyoto cell line; and M. Bassik, G. Brar, V. Denic, A. Frost, N. Ingolia, E. Quan, B. Toyama and other members of the Weissman laboratory for discussions. This work was supported by funding from Deutsche Forschungsgemeinschaft SFB/TR 13 projects A1 (K.S.) and D1 (A.S.), EUFP6 PRISM (K.S.), ETH Zurich (R.A.), the National Heart, Lung, and Blood Institute, National Institute of Health (N01-HV-28179) (R.A.), SystemsX.ch, the Swiss initiative for systems biology (R.A.), the Boehringer Ingelheim Fonds and the Swiss National Science Foundation (B.B.), the Howard Hughes Medical Institute (J.S.W.), the University of California, San Francisco Strategic Asthma Basic Research Center (J.S.W.), the National Science Foundation Graduate Research Fellowship Program (D.K.B.) and the Fannie and John Hertz Foundation (D.K.B.).

Author Contributions D.K.B. designed, performed and interpreted experiments. S.R.C. oversaw E-MAP data collection and analysis. B.B. performed and analysed protein mass spectrometry experiments to identify sites of phosphorylation under the supervision of R.A. C.S.E. performed and analysed lipidomic measurements with the support of A.S. and K.S. J.S.W. designed and interpreted experiments. D.K.B. and J.S.W. prepared the manuscript.

Author Information Reprints and permissions information is available at www.nature.com/reprints. The authors declare no competing financial interests. Correspondence and requests for materials should be addressed to J.S.W. (weissman@cmp.ucsf.edu).

METHODS

Growth media, plasmids and strain construction. All yeast experiments were conducted in strain BY4741 (ATCC), a related strain suitable for E-MAP experiments[27], and derivatives thereof. Strains were grown in YEPD media or media supplemented with myriocin (Sigma Aldrich; at least 12 h growth in myriocin in all cases), with the exception of samples prepared for lipidome analysis, which were grown in synthetic defined media.

Deletion, DAmP, overexpression (*pTEF2* and *pTHD3*), mCherry fusion and tetracycline-repressible promoter strains were constructed by standard PCR-based methods (see Supplementary Information). Strains expressing N-terminally epitope-tagged or GFP-tagged forms of wild-type and mutant Orm1, Orm2, Lcb1 and Sac1 were made by integration of DNA fragments encoding these gene variants into strains in which these genes had been deleted with the *URA3* counter-selectable marker. For the essential gene *LCB1*, a diploid strain was used for integration of the tagged allele containing the 3×Flag epitope inserted between codons 9 and 10, as previously reported[47]. *ORM1* and *ORM2* mutants, as well as the previously described *sac1–8* mutation[34], were created by standard PCR mutagenesis.

HEK293T cells (ATCC) and HeLa-Kyoto cells (a gift from A. Hyman) were grown in DMEM high-glucose media supplemented with penicillin, streptomycin, glutamine and 10% heat-inactivated fetal calf serum. *ORMDL3* was cloned from HEK293T cDNA into expression plasmids containing N- or C-terminal 3×Flag epitopes (p3XFLAG-CMV-10 and p3XFLAG-CMV-14; Sigma Aldrich).

E-MAP data collection and analysis. E-MAP data were collected and analysed as described previously[27] (manuscript in preparation). Genetic interaction patterns were compared for pairs of mutants by first identifying those genetic backgrounds for which E-MAP data were available for both mutants of interest. The similarity of the genetic interaction scores for the two mutants was then calculated by computing the cosine correlation between their interaction scores across these shared mutant backgrounds. For a given mutant of interest such as *orm2*Δ, these pairwise comparisons were performed with all other mutant strains having at least 200 shared genetic interaction data points. For the *ORM1* and *ORM2* overexpression mutants, an average of the *pTDH3* and *pTEF2* interaction profiles was used as the query profile for correlation calculations.

Lipidome analysis by mass spectrometry. Lipidome analyses were conducted as described previously[30] with minor modifications based on an existing method[48] for LCB analysis. Samples were collected from 20-ml cultures of yeast cells growing logarithmically in synthetic defined media or from about 4×10^6 to 6×10^6 HeLa cells grown as described earlier. Cells were washed in water or 155 mM ammonium bicarbonate at 4 °C, and cell pellets were then frozen immediately in liquid nitrogen. Yeast data are from two independent samples each analysed twice; HeLa cell data are from samples analysed in triplicate.

Growth rate measurements. Logarithmic growth rates were measured by OD_{600} from $n \geq 3$ replicate samples. Saturated cultures of the relevant strains were diluted into fresh media and grown for more than 7 h before growth analysis. Myriocin-treated cultures were grown for 3 h in the presence of the drug before analysis of growth rate.

Native affinity purifications of solubilized membrane proteins (large scale, yeast). ER-derived microsomes were prepared from yeast cells grown in YEPD (~4,000 OD_{600} units collected at OD_{600} ~1.4). Cells were collected, washed in water at 4 °C, resuspended in lysis buffer (50 mM HEPES-KOH, pH 6.8, 150 mM potassium acetate (KOAc), 2 mM MgOAc, 1 mM $CaCl_2$, 200 mM sorbitol) supplemented with protease inhibitors (Complete EDTA-free Cocktail; Roche) and frozen in a drop-by-drop fashion in liquid nitrogen. Frozen cells were then pulverized in a ball mill (6 × 3 min at 30 Hz; Retsch), thawed in lysis buffer at 4 °C and dounced ten times to homogeneity. After clarification by two consecutive centrifugations at 1,000*g*, microsomes were pelleted at 44,000*g*, resuspended in 0.5 ml lysis buffer and then diluted with 14 ml immunoprecipitation buffer (50 mM HEPES-KOH, pH 6.8, 150 mM KOAc, 2 mM MgOAc, 1 mM $CaCl_2$, 15% glycerol) with 2% digitonin (Calbiochem) supplemented with protease inhibitors. After nutating for 1.5 h at 4 °C, unsolubilized material was removed by centrifugation at 44,000*g*, and the remaining supernatant was added to anti-Flag resin (150 µl bed volume; Sigma Aldrich). Immunoprecipitations were nutated for 3 h at 4 °C and then washed 4 × 10 ml with immunoprecipitation buffer with 0.1% digitonin. Bound proteins were eluted twice with 150 µl immunoprecipitation buffer with 0.25% digitonin and 2 mg ml^{-1} 3×Flag peptide (Sigma Aldrich). Eluates were combined, separated on SDS–PAGE gels and stained with a colloidal blue staining kit (Invitrogen). Samples were prepared for phospho-site mapping using the same protocol, except that phosphatase inhibitors (Halt Phosphatase Inhibitor Cocktail; Pierce) were included in the buffers used.

Native affinity purifications of solubilized membrane proteins (small scale, yeast). Lysates for small-scale immunoprecipitations were prepared from logarithmically growing yeast cells (~25 OD_{600} units) grown in YEPD. Cultures were collected, washed in water at 4 °C and resuspended in 500 µl immunoprecipitation buffer (see above) with 0.1% digitonin and supplemented with protease and phosphatase inhibitors. Cell lysates were prepared by bead-beating at 4 °C, followed by addition of 500 µl immunoprecipitation buffer with 1.9% digitonin to raise the final digitonin concentration to 1%. Membrane proteins were solubilized by nutating lysates at 4 °C for 40 min. Unsolubilized material was next removed by centrifugation at 100,000*g*, and clarified lysates were incubated with anti-Flag resin (25 µl bed volume) for 2.5 h. The anti-Flag resin was then washed four times with 1 ml immunoprecipitation buffer containing 0.1% digitonin, and bound proteins were eluted by addition of 30 µl immunoprecipitation buffer with 0.25% digitonin and 2 mg ml^{-1} 3×Flag peptide.

Native affinity purifications of solubilized membrane proteins (small scale, human cells). HEK293T cells grown in DMEM high-glucose media supplemented with penicillin, streptomycin, glutamine and 10% heat-inactivated fetal calf serum were transfected using Fugene6 transfection reagent (Roche) according to the manufacturer's instructions. After approximately 48 h growth, transfected cells were collected by trypsinization and washed with PBS. Cell pellets were then resuspended at 4 °C in 1 ml immunoprecipitation buffer (see above) with 2% digitonin and protease inhibitors and nutated for 45 min to solubilize membrane proteins. Insoluble material was removed by centrifugation at 100,000*g*, and the clarified supernatant was incubated with anti-Flag resin (25 µl bed volume) for 2.5 h. The remainder of the immunoprecipitation was done in the same fashion as the yeast small-scale affinity purifications (see earlier).

Denaturing immunoprecipitations and phosphatase treatment. A 50-ml yeast culture in logarithmic phase growth was collected and resuspended in 10 ml 5% tricholoroacetic acid (TCA) and incubated for 10 min at 4 °C. Cell pellets were washed once in 1 ml 5% TCA, washed twice in 1 ml acetone and then air-dried. Acid-washed glass beads (200 µl) and 150 µl SDS lysis buffer (50 mM Tris-Cl, pH 7.8, 1 mM EDTA, 1% SDS, 2 M urea) supplemented with protease inhibitors were added to the dried pellets, which were then lysed by bead-beating (3 × 60 s at 4 °C). Lysates were diluted by addition of 1,350 µl Tween immunoprecipitation buffer (100 mM Tris-Cl, pH 7.8, 200 mM NaCl, 0.5% Tween-20, also supplemented with protease inhibitors) and clarified at 20,000*g*. Supernatants were then added to anti-Flag agarose (25 µl bed volume) and immunoprecipitated for 2.5 h at 4 °C. The anti-Flag resin was then washed 2 × 1 ml with Tween immunoprecipitation buffer, 1 × 1 ml with Tween/urea wash buffer (100 mM Tris-Cl, pH 7.8, 100 mM NaCl, 0.5% Tween-20, 2 M urea), and 2 × 1 ml in phosphatase buffer (NEBuffer 3; New England Biolabs), with 0.1% Tween-20. The washed resin was then resuspended in 54 µl phosphatase buffer plus 6 µl calf intestine phosphatase (New England Biolabs) and incubated for 1 h at 37 °C. After phosphatase treatment, the resin was sequentially washed with 1 ml Tween immunoprecipitation buffer and 1 ml SDS–DOC wash buffer (50 mM Tris-Cl, pH 7.8, 0.1% SDS, 0.1% Na-deoxycholate). Bound proteins were then eluted by addition of 60 µl SDS buffer (100 mM Tris-Cl, pH 6.8, 4% SDS, 20% glycerol) and incubation for 10 min at 65 °C.

RNA interference in HeLa cells. HeLa cells grown in DMEM high-glucose media supplemented with penicillin, streptomycin, glutamine and 10% heat-inactivated fetal calf serum were transfected using HiPerFect transfection reagent (Qiagen) according to the manufacturer's instructions. After approximately 72 h growth, transfected cells were collected by trypsinization for lipidomic and gene expression analysis. For each targeted gene, a pool of four siRNAs was used (ON-TARGETplus SMARTpool; Dharmacon), with siRNA sequences as follows: *ORMDL1*: 5′-UGGCAAGUUUCUAUACGAA-3′, 5′-GGAGUUGGCUUGCUUCAUA-3′, 5′-GCUUAUAAGUUAAAGGGCA-3′, 5′-GGACCAGCUUAACUUAUAA-3′; *ORMDL2*: 5′-UGGUAGGAUUGCUGCAUAU-3′, 5′-AGUUUAAUCAGGAUGGGUA-3′, 5′-GUGUACUGCUGCCGAAGUU-3′, 5′-AGUAUGAUGCUGCGCACUU-3′; *ORMDL3*: 5′-GAACAUGGACCACGCAGUU-3′, 5′-ACACUAAGUACGACCAGAU-3′, 5′-CGGUACGGCUUCUGGAUUG-3′, 5′-UGGGUAGGGAGCUGUCUAA-3′.

RT–PCR analysis of gene expression in HeLa cells. RNA was extracted from HeLa cells using the RNeasy kit (Qiagen) after cell homogenization (QIAshredder; Qiagen). Extracted RNA was reverse-transcribed using AMV RT (Promega) and amplified with Taq polymerase (GoTaq; Promega). Real-time SYBR green fluorescence was monitored using a DNA Engine Opticon System (MJ Research), and the following primers were used: *RPL19*: 5′-ATGTATCACAGCCTGTACCTG-3′, 5′-TTCTTGGTCTCTTCCTCCTTG-3′; *ORMDL1*: 5′-CTGACCAGGGTAAAGCAAGG-3′, 5′-TCCAAAGATCCGAACACCAT-3′; *ORMDL2*: 5′-CATACGGTGAAAGGGACACC-3′, 5′-CGGCAGCAGTACACTTAGCA-3′; *ORMDL3*: 5′-AACCCCTGCTCACTTGTTTG-3′, 5′-CAAAGACCCATCCCACACTT-3′.

Live-cell yeast fluorescence microscopy. Yeast cells expressing Sec63–mCherry and GFP–Orm1 or GFP–Orm2 were grown in rich media with or without myriocin and spotted on a concanavalin-A-coated 25 × 50 mm coverslip covered with a 22 × 22 mm coverslip. Cells were imaged through the 25 × 50 mm coverslip using a Zeiss Axiovert 200M microscope (Carl Zeiss Microimaging) equipped

with a spinning disk confocal scanhead and laser system (Yokogawa CS10, Yokogawa Electronics; Solamere). Images were collected as Z-stacks with 0.5 μm spacing between frames using μManager software and an ImagEM C9100-13 EM-CCD camera (Hamamatsu Photonics).

Serial-dilution cell-spotting assays. Logarithmically growing yeast were spotted onto agar plates in tenfold serial dilutions from a starting OD_{600} density of 0.3 to a final OD_{600} density of 3×10^{-4}. Plates were imaged after growth for 24–48 h. Plates with myriocin were standard YEPD supplemented with 0.1% tergitol and 2 mM citric acid.

LCB extraction and analysis by high-performance liquid chromatography. LCB extraction and analysis was performed as described[48]. Myriocin-treated samples were grown for 14–16 h in the presence of drug before extractions. For extractions, 50 ml of a logarithmically growing culture was collected and resuspended in 10 ml 5% TCA at 4 °C. After a 10 min incubation, cells were washed once in 5% TCA and three times in H_2O at 4 °C. Cell pellets were then resuspended in 75 μl H_2O followed by addition of 425 μl 70.6 mM TEA/ethanol. Lipids were extracted by bath sonication (3 × 99 s, 30 W) and incubation at 65 °C for 30 min. Of this extract, 150 μl was derivatized by reaction for 40 min at room temperature with 30 μl of AccQ Fluor reagent (Waters Corporation). Ester-linked lipids were de-acylated by addition of 22.5 μl of 1.5 M KOH/methanol. After 30 min incubation at 37 °C, the reaction was neutralized by addition of 22.5 μl 1.74 M acetic acid/methanol. Samples were analysed on an Agilent Chemstation high-performance liquid chromatography using a reverse-phase C18 column (ZORBAX Eclipse XDB-C18; Agilent).

Protein identification by mass spectrometry. Gel slices were trypsinized and mass spectra were acquired on a Bruker Reflex III MALDI-TOF mass spectrometer. Proteins were identified by searching the NCBInr database using the MS-Fit program on Protein Prospector (University of California, San Francisco, http://prospector.ucsf.edu)[49].

Identification of phosphorylation sites by mass spectrometry. Proteins eluted from native affinity purifications of 3×Flag–Orm1 or 3×Flag–Orm2 (see earlier) were precipitated using ice-cold acetone. After incubation overnight at −20 °C, proteins were pelleted at 4 °C by centrifugation. Protein pellets were then processed, and the resulting peptide mixtures were analysed on a hybrid LTQ-Orbitrap mass spectrometer, as described previously[50]. Database searches were performed using the Saccharomyces Genome Database non-redundant database, as described[50].

47. Gable, K., Slife, H., Bacikova, D., Monaghan, E. & Dunn, T. M. Tsc3p is an 80-amino acid protein associated with serine palmitoyltransferase and required for optimal enzyme activity. *J. Biol. Chem.* **275,** 7597–7603 (2000).
48. Lester, R. L. & Dickson, R. C. High-performance liquid chromatography analysis of molecular species of sphingolipid-related long chain bases and long chain base phosphates in *Saccharomyces cerevisiae* after derivatization with 6-aminoquinolyl-N-hydroxysuccinimidyl carbamate. *Anal. Biochem.* **298,** 283–292 (2001).
49. Jiménez, C. R., Huang, L., Qiu, Y. & Burlingame, A. L. in *Current Protocols in Protein Science* (eds Coligan, J. E., Dunn, B. M., Ploegh, H. L., Speicher, D. W. & Wingfield, P. T.) 16.4.1–16.4.5 (John Wiley, 1998).
50. Huber, A. *et al.* Characterization of the rapamycin-sensitive phosphoproteome reveals that Sch9 is a central coordinator of protein synthesis. *Genes Dev.* **23,** 1929–1943 (2009).